bon-oxygen double bond. The carbonyl ligands possess carbon-oxygen triple bonds with an average value of 1.16 Å.

**Acknowledgment.** Financial support of this research by the National Science Foundation (Grant CHE 88-17873) and the Robert A. Welch Foundation is greatly appreciated.

**Registry No.** I, 106162-73-6; II, 121918-96-5; III, 106162-80-5; [PPN][OPh], 121888-64-0; $[Et_4N][OPh]$, 32580-85-1; $[Et_4N][OC_6H_4CH_3$-*m*], 121888-65-1; $[Et_4N][Cr(CO)_5OPh]$, 121918-63-6; $Cr(CO)_6$, 13007-92-6; $Cr(CO)_5THF$, 15038-41-2; $[Et_4N][Cr(CO)_5COOPh]$, 121918-65-8; $[Et_4N][Cr_4(CO)_{12}(OPh)_4]$, 97879-19-1; $W(CO)_5THF$, 36477-75-5; $W(CO)_6$, 14040-11-0; $[Et_4N][W(^{13}CO)_5OPh]$, 121918-67-0; [PPN][W(CO)$_5$OPh], 121918-68-1; $[Et_4N][W(CO)_5COOPh]$, 121918-69-2; $[Et_4N][W_4(CO)_{12}(OPh)_4]$, 106191-48-4; $[Et_4N][cis$-$Cr(CO)_4(PMe_3)OPh]$, 121918-71-6; $[Et_4N][cis$-$Cr(CO)_4(P(OMe)_3)OPh]$, 121918-73-8; $[Et_4N][cis$-$W(CO)_4(PMe_3)OPh]$, 121918-75-0; $[Et_4N][cis$-$W(CO)_4(P(OMe)_3)OPh]$, 121918-77-2; $[Et_4N][cis$-$W(CO)_4(PPh_3)OPh]$, 121918-79-4; $[Et_4N][Cr(CO)_5O_2COPh]$, 121918-81-8; $[Et_4N][Cr(CO)_5SC(O)OPh]$, 121918-83-0; $[Et_4N[[Cr(CO)_5S_2COPh]$, 121918-85-2; $[Et_4N][W(CO)_5O_2COPh]$, 121918-86-3; $[Et_4N][W(CO)_5O_2COC_6H_4CH_3$-*m*], 121918-87-4; $[Et_4N][W(CO)_5OC_6H_4CH_3$-*m*], 106162-75-8; $[Et_4N][W(CO)_5SC(O)OPh]$, 121918-89-6; $[Et_4N][W(CO)_5S_2COPh]$, 121918-91-0; $[Et_4N]_2[W(CO)_4CO_3]$, 106162-79-2; $[Et_4N]_2[W(CO)_4(CO_2S)]$, 121918-93-2; $[Et_4N]_2[W(CO)_4S_2CO]$, 121918-95-4; $CO_2$, 124-38-9; COS, 463-58-1; $CS_2$, 75-15-0; phenol, 108-95-2.

**Supplementary Material Available:** Drawing with the labeling scheme for the $[Et_4N]^+$ cations in $[Et_4N][W(CO)_5OPh\cdot0.5H_2O]$ (II, Figure 1S), figure of the unit cell of $[Et_4N][W(CO)_5OPh]$ (Figure 2S), figure of the unit cell of $[Et_4N][W(CO)_5OPh\cdot0.5H_2O]$ (Figure 3S), table of infrared spectral data for the complexes $[Et_4N][M(CO)_5OR]$ in THF (Table 1S), tables of atomic coordinates for $[Et_4N][W(CO)_5OPh]$ (I, Table 2S), $[Et_4N][W(CO)_5OPh\cdot0.5H_2O]$ (II, Table 3S), and $[Et_4N]_2[W(CO)_3\cdot H_2O]$ (III, Table 4S), tables of anisotropic thermal parameters for I (Table 5S), II (Table 6S), and III (Table 7S), H atom coordinates and isotropic thermal parameters of I (Table 8S), II (Table 9S), and III (Table 10S) (12 pages); listing of calculated and observed structure factor amplitudes for I (Table 11S), II (Table 12S), and III (Table 13S) (55 pages). Ordering information is given on any current masthead page.

# X-ray Absorption Edge and EXAFS Study of the Copper Sites in ZnO Methanol Synthesis Catalysts

**Lung-Shan Kau, Keith O. Hodgson,* and Edward I. Solomon***

*Contribution from the Department of Chemistry, Stanford University, Stanford, California 94305.* *Received August 15, 1988*

**Abstract:** X-ray absorption edge and EXAFS data are presented for the binary form of the Cu-ZnO methanol synthesis catalysts. For the calcined catalyst, a significant amount of the Cu(II) is found to be doped into the tetrahedral sites of the ZnO lattice based on a quantitative analysis of X-ray absorption difference edges. Alternatively, the EXAFS spectra exhibit less evidence for this Cu(II)/ZnO site, which is attributed to disorder effects on the outer-shell Cu-Zn EXAFS. A quantitative analysis of the EXAFS for the reduced catalyst demonstrates that it contains metallic Cu, small Cu clusters, and a Cu oxide phase. Analysis of the X-ray absorption edges of the reduced catalyst shows that this oxide phase contains both $Cu_2O$ and tetrahedral Cu(I) sites. Thus, the dispersed phase in the methanol synthesis catalyst, which corresponds to ~50% of the Cu, consists of both a small Cu cluster component and Cu(I) doped into the ZnO lattice.

ZnO is an effective catalyst for the hydrogenation of CO to $CH_3OH$. The active high-temperature, high-pressure catalyst also contains either $Al_2O_3$ or $Cr_2O_3$, which acts as an intercrystalline promoter to inhibit sintering of ZnO crystallites,[1] with ZnO being the active phase. The chemisorption properties of CO on the four chemically different, low index surfaces of ZnO have been defined in detail by using angle-resolved photoelectron and high-resolution electron energy loss spectroscopies.[2] These studies show that CO binds carbon end down to the coordinatively unsaturated Zn(II) on terrace and step sites, depending on the surface.

The catalytic activity of ZnO for methanol synthesis can be strongly enhanced by the addition of a small amount of Cu. Binary Cu/ZnO is a low-temperature, low-pressure catalyst[3] which is obtained by reduction of CuO/ZnO. The maximum rate of methanol synthesis appears at catalyst compositions near a CuO:ZnO ratio of 30:70. The Cu component is thought to act as an intracrystalline promoter that significantly lowers the activation barrier for the reaction (from ~30 to 18 kcal/mol).[4] The presence of a small amount of $CO_2$ in the feed gas is required to prevent catalyst deactivation. While there have been a number of investigations of the mechanism of methanol synthesis on the Cu/ZnO heterogeneous catalyst and of the $CO_2$ promotion effect, these are still not well understood.

Recent studies have demonstrated that the reduced catalyst contains, in addition to the ZnO and metallic Cu, a significant amount of the Cu in a dispersed phase. Using a combination of techniques (X-ray photoelectron spectroscopy (XPS), Auger, scanning transmission electron microscopy and surface area measurements), Klier et al.[5] concluded for the activated catalyst

(1) (a) Natta, G. *Catalysis* **1955**, *3*, 349. (b) Burzyk, J.; Haber, J. *Bull. Acad. Pol. Sci. Ser. Sci. Chim.* **1969**, *17*, 531. (c) *Ibid.* 539. (d) Burzyk, J.; Haber, J.; Nowotny, J. *Ibid.* 543.

(2) (a) D'Amico, K. L.; McFeely, F. R.; Solomon, E. I. *J. Am. Chem. Soc.* **1983**, *105*, 6380. (b) D'Amico, K. L.; Trenary, M.; Shinn, N. D.; Solomon, E. I.; McFeely, F. R. *J. Am. Chem. Soc.* **1982**, *104*, 5102. (c) Gay, R. R.; Nodine, M. H.; Henrich, V. E.; Zeiger, H. J.; Solomon, E. I. *J. Am. Chem. Soc.* **1980**, *102*, 6752.

(3) Klier, K. *Adv. Catal.* **1982**, *31*, 243, and references therein.

(4) Emmett, P. H. In *Catalysis Then and Now*; Emmett, P. H., Sabbatier, P., Reid, E. E., Eds.; Franklin Publishing: Englewood, NJ, 1965; Part I, pp 173.

(5) (a) Parris, G. E. Ph.D. Thesis, Lehigh University, 1982. (b) Dominiquez, J. M.; Simmons, G. W.; Klier, K. *J. Mol. Catal.* **1983**, *20*, 369. (c) Klier, K.; Chatikavanij, V.; Herman, R. G. *J. Catal.* **1982**, *74*, 343. (d) Metha, S.; Simmons, G. W.; Klier, K.; Herman, R. G. *J. Catal.* **1979**, *57*, 339. (e) Bulko, J. B.; Simmons, G. W.; Klier, K.; Herman, R. G. *J. Phys. Chem.* **1979**, *83*, 3118. (f) Herman, R. G.; Klier, K.; Simmons, G. W.; Finn, B. P.; Bulko, J. B.; Kobylinske, T. P. *J. Catal.* **1979**, *56*, 407.

0002-7863/89/1511-7103$01.50/0 

that up to 50% of the Cu is dissolved in ZnO. Diffuse reflectance spectra on these activated catalysts exhibit a characteristic near-infrared (IR) absorption feature that was attributed to the highly dispersed phase containing Cu(I) substituted for Zn(II) in the tetrahedral sites of the wurtzite lattice. The Cu(I) ion was considered to chemisorb and activate the CO with $H_2$ being activated by the ZnO. In addition, Klier et al. also noted that reduced pure $Cu_2O$ had no observable activity for methanol synthesis.[5f]

Okamoto et al.[6] employed XPS to study the Cu phase on the surface and concluded that a two-dimensional Cu(0)–Cu(I) species was responsible for catalytic activity. In contrast, a number of authors have proposed that hydrogenation of $CO_2$ predominates and that metallic Cu is the active component.[7] Recently, Baussart et al.[8] studied the selective hydrogenation of $CO_2$ to $CH_3OH$ by the low-pressure Cu/Zn/Al catalyst (using X-ray powder diffraction, diffuse reflectance, and gas chromatography) and concluded that the presence of $Cu_2O$ correlates with higher selectivity of the catalyst. Thus, there is still controversy about the nature of the dispersed phases and the types of Cu-active sites present.

X-ray absorption edge and extended fine structure (EXAFS) spectroscopy is a particularly useful technique for providing molecular level structural information in dispersed and amorphous materials.[9] Analysis of the EXAFS region provides information about the distances, numbers, and types of neighboring atoms surrounding the absorber.[10] Recently, EXAFS studies have been used in several investigations of the Cu-active site in reduced Cu/ZnO catalysts. With Cu catalysts (~30 wt %) activated by reducing gas, highly dispersed Cu clusters have been observed[11,12] which reversibly aggregate with heating cycles in an $H_2$ stream.[13] Relatively low-resolution EXAFS data, collected by using a rotating anode X-ray generator, have been analyzed to suggest that three components (metallic Cu, a $Cu_2O$-like phase, and Cu(I) in interstitial sites in the ZnO lattice) were present in the reduced catalyst.[14]

For the calcined catalysts, Klier et al.[5b,d] reported the presence of crystallites of CuO and ZnO, as well as several percent of CuO dissolved in ZnO. Okamoto et al.[6] concluded that, for the low Cu content (<30%) calcined catalyst, three types of Cu species (crystalline CuO, amorphous CuO, and Cu(II) dissolved in ZnO) exist on the surface of the catalyst. From high-quality X-ray absorption spectroscopy (XAS) studies at liquid nitrogen temperature, Clausen et al.[12] reported that only a CuO phase was present with no evidence of Cu doping into the ZnO lattice. In the rotating anode EXAFS study of the calcined form mentioned above, Rao et al.[14] concluded that both Cu(II) in a CuO-like phase and Cu(II) occupying substitutional sites in the ZnO lattice are present.

The absorption edge region contains transitions that reflect the electronic structure of the absorbing atom.[15,16] While the analysis of X-ray absorption edge data is generally less developed than for EXAFS, recent work on Cu edges provides a useful approach toward defining the electronic structure of these sites in catalysts.[16] From systematic studies on Cu model complexes, correlations have been developed between edge features and geometric and electronic structure. The edges of 2- and 3-coordinate Cu(I) complexes have absorption features at energies below 8985 eV that can be assigned as 1s → 4p transitions. For 4-coordinate tetrahedral Cu(I) complexes, the 1s → 4p transitions are all above 8985 eV. Cu(II) compounds do not show edge absorption features below 8985 eV, except for a well-separated, weak 8978-eV absorption feature, which is the 1s → 3d transition.[16c] With increasing tetrahedral distortion, the intensity of this 8978-eV transition increases due to Cu 4p–3d mixing. For the tetragonal Cu(II) complexes, there is an additional intense transition at 8986 eV which has been assigned as the 1s → $4p_z$ plus ligand-to-Cu(II) charge-transfer shakedown. This shakedown transition shifts to higher energy with increasing tetrahedral distortion.[16b]

The goal of the work presented here has been to use X-ray absorption edge and EXAFS methods to determine and quantitate the different Cu phases present in methanol synthesis catalysts on a molecular level. Although the 30/70 Cu/ZnO catalyst has the highest activity and exhibits the most intense near-IR absorption feature, it contains ~50% of the Cu in the form of large metallic Cu particles and thus EXAFS studies of these catalysts have detected only the presence of Cu metal.[11] More tractable systems, which contain 10% or less Cu, also show a near-IR absorption feature and are active catalysts.[5] The low-percent Cu/ZnO catalysts permit detailed spectroscopic characterization of the dispersed Cu with less interference from Cu metal. We have collected XAS data at higher resolution on these low-percent Cu-doped catalysts and have analyzed these data in detail. We have studied, as a function of weight percent Cu, the calcined and reduced catalysts. From these studies, we have characterized the types of Cu sites present in the dispersed phase of the heterogeneous Cu/ZnO catalysts. In the following paper,[17] we further define the surface dependence of these Cu sites and their reactivity with CO through parallel studies of dispersed Cu sites on single crystal ZnO surfaces in ultrahigh vacuum.

## Experimental Section

Cu metal foil was obtained from Goodfellow Ltd., England, and $Cu_2O$ and CuO from Aldrich Chemical Co. ZnO was obtained from the New Jersey Zinc Co. The 0.5%, 1%, 5%, and 10% (wt % Cu) calcined binary CuO/ZnO catalyst samples were prepared and characterized by Haldor Topsoe A/S, Denmark, using published procedures.[12] The CuO/ZnO catalysts (1%, 5%, and 10%) were activated at 493 K under a steady flow of gas composed of 4% $CO_2$/0.5% CO/2.25% $H_2$/93.25% $N_2$/saturated $H_2O$ for 4–8 h. Following activation, the samples were cooled to ambient temperature under a steady flow of $N_2$. Samples were prepared for XAS measurements in a high-purity (<1 ppm $O_2$) inert $N_2$ atmosphere box. Each sample was mixed with BN and then pressed into a homogeneous pellet in an aluminum frame sample cell that was covered with Mylar film as windows. For measurement, the Mylar-protected, mounted samples were transferred in an Ar-filled glovebag into an inert-atmosphere XAS sample compartment that was purged with He throughout the measurements.

Cu K-edge XAS data were collected at the Stanford Synchrotron Radiation Laboratory wiggler beam lines 4-2 and 7-3 using dedicated beam at 3.0 GeV, ~50 mA. The radiation was monochromatized by a Si(220) two-crystal monochromator. Internal Cu foil energy calibration was performed by assigning the first inflection point of Cu foil at the K absorption edge as 8980.3 eV.[18] In conversion of energy to $k$ space ($k^2$

(6) (a) Okamoto, Y.; Fukino, K.; Imanaka, T.; Teranishi, S. *J. Phys. Chem.* **1983**, *87*, 3740. (b) *Ibid.* 3747.

(7) (a) Andrew, S. P. S. Plenary Lecture (Paper 12), Post Congress Symposium, 7th International Congress on Catalysis, Osaka, 1980. (b) Chinchen, G. C.; Parker, D. G.; Short, F. D.; Spencer, M. S.; Waugh, K. C.; Whan, D. A. *Prepr. Pap.—Am. Chem. Soc., Div. Fuel Chem.* **1984**, *29*, 178.

(8) Baussart, H.; Delobel, R.; Le Bras, M.; Le Maguer, D.; Leroy, J. *App. Catal.* **1985**, *14*, 381.

(9) (a) Lytle, F. W.; Via, G. H.; Sinfelt, J. H. In *Synchrotron Radiation Research*; Winick, H., Doniach, S., Eds.; Plenum Press: New York, 1980; Chapter 12. (b) Via, G. H.; Sinfelt, J. H.; Lytle, F. W. In *EXAFS Spectroscopy; Techniques and Applications*; Teo, B. K., Joy, D. C., Eds.; Plenum Press: New York, 1981; p 159.

(10) (a) Cramer, S. P.; Hodgson, K. O. *Prog. Inorg. Chem.* **1979**, *25*, 1. (b) Lee, P. A.; Citrin, P. H.; Eisenberger, P.; Kincaid, B. M. *Rev. Mod. Phys.* **1981**, *53*, 769. (c) Teo, B. K. *EXAFS: Basic Principles and Data Analysis*; Springer-Verlag: New York, 1986. (d) Scott, R. A. *Methods Enzymol.* **1985**, *117*, 414. (e) Cramer, S. P. In *X-ray Absorption Spectroscopy*; Koningsberger, D. C., Prins, R., Eds.; Wiley: New York, 1988; Chapter 7.

(11) Vlaic, G.; Bart, J. C. J.; Cavigiolo, W.; Pianzola, B.; Mobilio, S. *J. Catal.* **1985**, *96*, 314.

(12) (a) Clausen, B. S.; Lengeler, B.; Rasmussen, B. S. *J. Phys. Chem.* **1985**, *89*, 2319. (b) Clausen, B. S.; Lengeler, B.; Rasmussen, B. S.; Niemann, W.; Topsoe, H. *J. Phys. (Paris)* **1986**, *C8*, 237.

(13) Togji, K.; Udagawa, Y.; Mizushima, T.; Ueno, A. *J. Phys. Chem.* **1985**, *89*, 5671.

(14) Sankar, G.; Vasudevan, S.; Rao, C. N. R. *J. Chem. Phys.* **1986**, *85*, 2291.

(15) Bianconi, A. In *X-ray Absorption Spectroscopy*; Koningsberger, D. C., Prins, R., Eds.; Wiley: New York, 1988; Chapter 11, and references therein.

(16) (a) Kau, L.-S.; Penner-Hahn, J. E.; Solomon, E. I.; Hodgson, K. O. *J. Phys. (Paris)* **1986**, *C8*, 1177. (b) Kau, L.-S.; Spira-Solomon, D. J.; Penner-Hahn, J. E.; Hodgson, K. O.; Solomon, E. I. *J. Am. Chem. Soc.* **1987**, *109*, 6433. (c) Hahn, J. E.; Scott, R. A.; Hodgson, K. O.; Doniach, S.; Desjardins, S. R.; Solomon, E. I. *Chem. Phys. Lett.* **1982**, *88*, 595.

(17) Didziulis, S. V.; Solomon, E. I. *J. Am. Chem. Soc.*, the following paper in this issue.

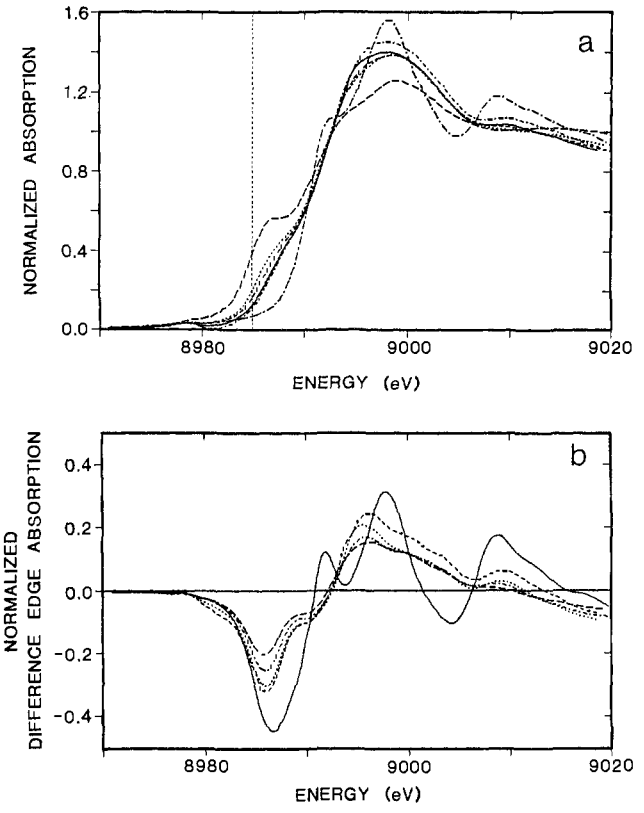


**Figure 1.** (a) Comparison of the X-ray absorption K edges for 0.5% (dot–short dash), 1% (solid), 5% (short dash), 10% (dot) calcined catalyst samples, CuO (long dash), and ZnO (dot–long dash). The vertical dotted line is at 8985 eV. The ZnO edge has been shifted by −674 eV such that the absorption maxima above the respective edges coincide. (b) Difference edge spectra where the CuO absorption edge has been subtracted from the energy-shifted ZnO edge (solid; both edges as shown in Figure 1a), from 0.5% (dash), 1% (dot), 5% (dot–dash), and 10% (long dash) Cu/ZnO calcined samples (all shown in Figure 1a).

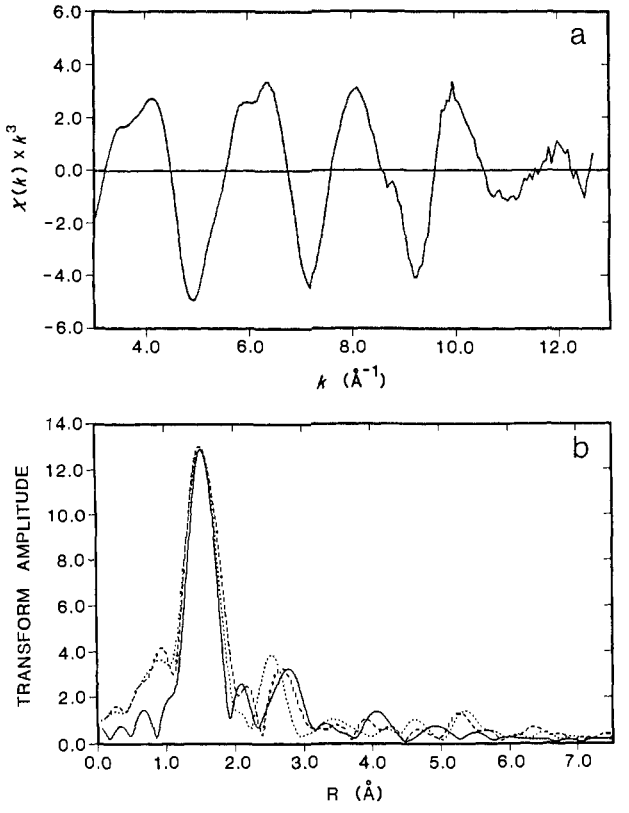


**Figure 2.** (a) Unfiltered EXAFS spectrum of the 1% calcined Cu/ZnO catalyst. (b) Fourier transforms of the EXAFS data over $k$ = 3.5–12.2 Å$^{-1}$ for 1% (solid), 5% (dash), and 10% (dot) calcined Cu/ZnO catalyst samples.

$= [2m_e(E - E_0)/\hbar^2])$, $E_0$ was defined as 9000 eV. EXAFS data up to ~650 eV above the K edge (i.e., to $k$ = 13 Å$^{-1}$) were recorded in transmission mode. Typically, 2–3 scans were collected for each sample, and a weighted average of all the acceptable data was then calculated to produce the final spectra. No changes in edge or EXAFS data were observed with time.

Reduction and analysis of the data were performed by using previously reported methods.[19] Briefly, this procedure involved background subtraction by means of a polynomial function and normalization. For edges, normalization was accomplished by fitting a straight line to the postedge region (9045–9600 eV) and normalizing the edge jump to 1.0 at 9000 eV. For EXAFS analysis, background subtraction was performed using a polynomial spline function. The spline points were adjusted to minimize the amplitude of the low-$R$ (<1 Å) features in the Fourier transform without affecting the other amplitudes. In all cases, refinement results were insensitive to the details of the several splines tested in calculating the reported EXAFS, and thus the results reported below are not artifacts of the final data reduction procedure. Fourier transforms were calculated by numerical integration using $k^3$-weighted EXAFS and a 0.1-Å Gaussian window (see Tables I–III for further details). Quantitative analyses of the EXAFS data were accomplished by using a nonlinear least-squares curve-fitting procedure. The parametrized amplitude and phase functions appropriate to the given absorber–scatterer pair were determined empirically.[19] Fits were carried out over the $k$ range 4–12 Å$^{-1}$.

## Results and Analysis

**(A) Calcined Samples.** Cu K-edge X-ray absorption spectra were collected for four calcined Cu/ZnO samples (0.5, 1, 5, and 10%, Figure 1). The presence of a weak feature at 8978 eV (1s → 3d transition) and the lack of an intense peak below 8985 eV both indicate that these samples contain predominantly Cu(II) (see ref 16). Insight into the geometry of this Cu(II) site can be obtained by comparison to the K-edge spectra of CuO and ZnO, the former being tetragonal and the latter being tetrahedral metal ion sites. The ZnO spectrum was overlayed by adjusting its energy so that the position of maximum absorption coincides with that of CuO (this requires an offset of the Zn edge by −674 eV). When compared to the CuO edge spectrum, the edge spectra of the catalysts show a more resolved 8978-eV feature and a much weaker 8986-eV shoulder and have a higher resonance feature at ~9000 eV. The latter two features look more like the edge spectrum of ZnO (note that ZnO can have no 1s → 3d transition as it is a $d^{10}$ ion). There is, however, a trend in the edge spectra for the higher Cu percentage catalyst samples to start approaching the edge spectrum of CuO. As described in the introduction, a strong 8978-eV feature in a Cu(II) edge spectrum indicates that a fraction of the Cu(II) ions in the calcined catalyst are in a site distorted toward a tetrahedral geometry. Further, the relatively low intensity of the 8986-eV feature also suggests a distortion of the Cu(II) sites away from tetragonal symmetry, as a decrease in 8986-eV intensity is also observed for ZnO and distorted tetrahedral Cu(II) model complexes.[20]

The trend in the edge spectra to approach that of CuO for the higher percentage calcined catalysts suggests that the calcined catalyst is composed of at least two components, CuO and Cu doped into ZnO. We have quantified the relative amount of Cu(II) in these phases by subtracting the normalized CuO edge from that of the energy-shifted edge of ZnO and from the normalized edges of the calcined samples. As CuO has a peak at 8986 eV and ZnO at ~9000 eV (after being shifted by −674 eV), this CuO–ZnO difference results in a negative feature at 8986 eV and a positive feature at ca. 9000 eV. The amplitudes of this standard can be compared with the amplitude of the 8986-eV

(18) Scott, R. A.; Hahn, J. E.; Doniach, S.; Freeman, H.; Hodgson, K. O. *J. Am. Chem. Soc.* **1982**, *104*, 5364.
(19) Cramer, S. P.; Hodgson, K. O.; Stiefel, E. I.; Newton, W. E. *J. Am. Chem. Soc.* **1978**, *100*, 2748.
(20) Smith, T. A. G. Ph.D. Thesis, Stanford University, Stanford, CA, 1985.

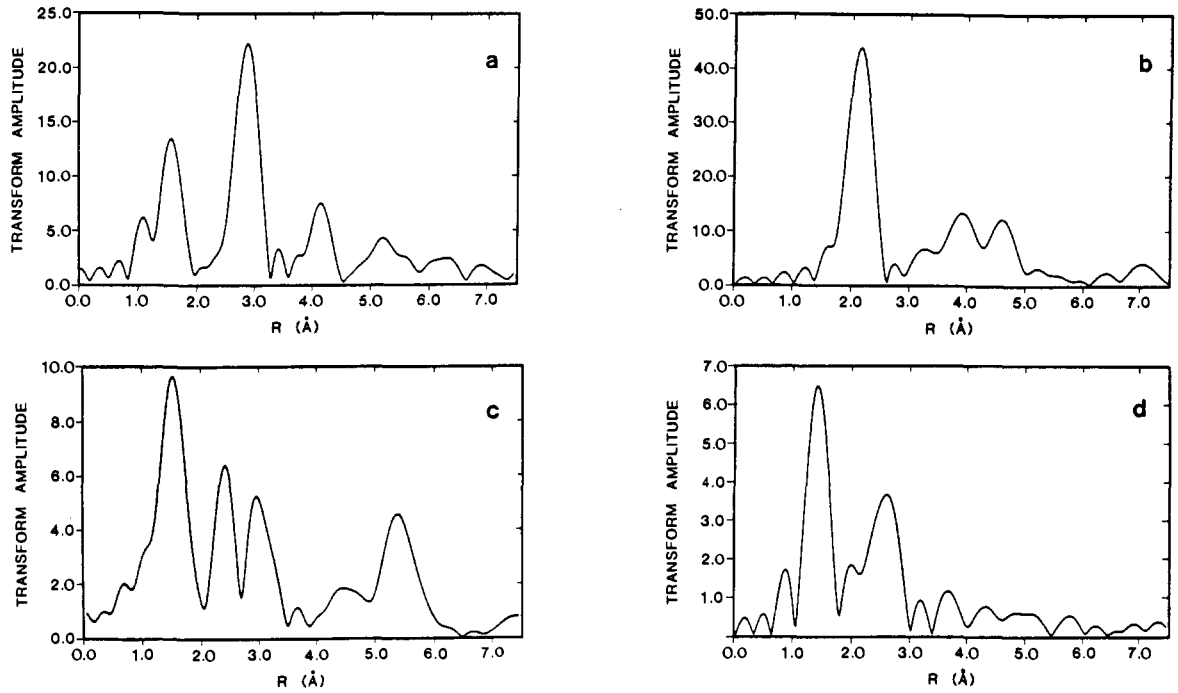


**Figure 3.** Fourier transforms of the EXAFS data over $k$ = 3.5–12.5 Å$^{-1}$ for (a) ZnO, (b) Cu metal, (c) CuO, and (d) $Cu_2O$.

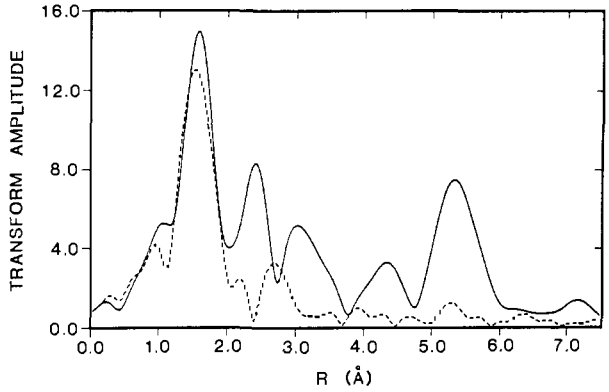


**Figure 4.** Fourier transforms of the EXAFS data over $k$ = 3.3–12.3 Å$^{-1}$ for the calcined 5% Cu/ZnO sample at room temperature (dash) and at 77 K (solid).

**Table I.** Curve-Fitting Results of Cu EXAFS Data for 1% Calcined Cu/ZnO Catalysts

| shells of backscatters | | |
|---|---|---|
| O[a] $R$, Å (CN) | ZnO2[b] $R$, Å (CN) | ZnO3[c] $R$, Å (CN) |
| 1.96 (4.7) | 3.29 (1.7) | 4.65 (1.7) |

[a] Curve fitting was to the Fourier-filtered first-shell EXAFS from the catalyst sample ($R$ = 0.9–2.1 Å, Gaussian window = 0.1), by using empirical Cu–O backscattering parameters. [b] Curve fitting was to the Fourier-filtered second-shell EXAFS of the catalyst sample ($R$ = 2.3–3.3 Å, Gaussian window = 0.1). The parameters used were taken from the second shell in the Fourier transform of ZnO which has 6 Zn at 3.21 Å and 6 Zn at 3.25 Å (average 12 Zn at 3.23 Å). [c] Curve fitting was to the Fourier-filtered third-shell EXAFS of the catalyst sample ($R$ = 3.7–4.4 Å, Gaussian window = 0.1). The parameters used were taken from the third shell in the Fourier transform of ZnO which contains 6 Zn at 4.57 Å and 6 O at 4.57 Å (average 12 atoms at 4.57 Å).

negative peak in the difference edge of each of the calcined samples in Figure 1b to quantify the amount of CuO phase present. Assuming that the remaining Cu is in tetrahedral sites, this analysis shows that, for 0.5, 1, 5, and 10% CuO/ZnO calcined samples, there is 75, 67, 55, and 47 ± 10% of Cu(II) substituted into Zn(II) sites in ZnO.

EXAFS data for the 1, 5, and 10% calcined samples were collected at room temperature (Figure 2a shows the data for the 1% sample). Fourier transforms (FT) are shown in Figure 2b. The FTs for the calcined catalyst EXAFS are quite different from that of CuO (compare to Figure 3c). In particular, the catalyst does not exhibit the strong outer-shell features present in the FT for CuO (peaks at 2.4, 3.0, and 5.4 Å). Further, the second peak in the FT of the 1% calcined catalyst at ~2.8 Å shifts to shorter distance as the Cu weight percent of the catalyst increases. EXAFS data for the 5% calcined sample were also collected at 77 K, and the FT of this data is compared with that of the room-temperature data in Figure 4. At low temperature, the outer-shell features analogous to those of CuO are clearly present. This indicates that, consistent with the edge analysis, there is also a CuO component in the calcined catalyst that becomes more prominent in the EXAFS FT at low temperature due to diminished Debye–Waller effects.

The FTs of the calcined samples (Figure 2b) can be compared with that of ZnO (Figure 3a). ZnO exhibits a particularly intense second-shell peak at about 2.8 Å (non-phase-shift corrected) due to 6 Zn at 3.21 Å and 6 Zn at 3.25 Å. There is an additional weaker 4.2 Å peak due to 6 Zn at 4.57 Å and 6 O at 4.57 Å. For the 1% calcined sample, there are weak features at around 2.8 and 4.2 Å in the FT of the EXAFS data that compare well with the peak positions in the FT of the ZnO EXAFS. However, the 2.8-Å peak in the catalyst is considerably weaker than that in ZnO. To interpret these outer-shell features in the 1% calcined sample, EXAFS curve-fitting analyses were performed, using empirical Zn-backscatterer parameter sets extracted from the second- and third-shell features of ZnO, by Fourier-filtering the individual components from the EXAFS data (Table I).

From these quantitative curve-fitting results, the second shell of the 1% catalyst was found to contain 1.7 rather than the 12 Zn atoms contributing to this peak in the pure ZnO EXAFS spectrum, which would indicate that only 14% of the Cu is in ZnO sites. However, from the difference edge analysis presented above, there should be about 67% Cu(II) in the ZnO lattice for the 1% CuO/ZnO sample. Thus the amplitude of the Cu in the ZnO lattice sites appears to be reduced by 14/67%. Two factors can contribute to this reduction. First, if most of these Cu ions are at the surface, the amount of second-shell Zn scattering should be decreased due to the lower outer-sphere coordination number of surface sites. This, however, can only reduce the intensity by $^{8}/_{12} \times 67\%$. The second and apparently dominant contribution

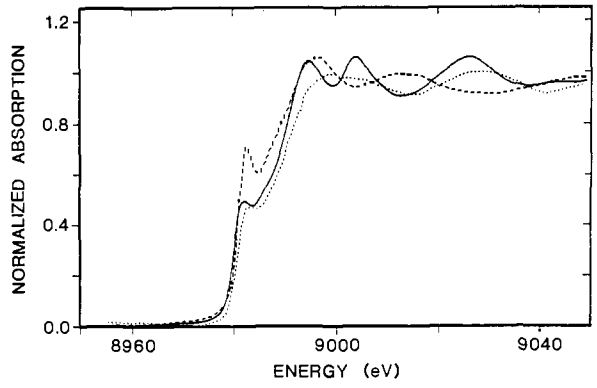


**Figure 5.** Cu X-ray absorption K edges for metallic Cu (solid), $Cu_2O$ (dash), and 10-Å Cu microclusters (dot). (The microcluster edge is reproduced from ref 21).

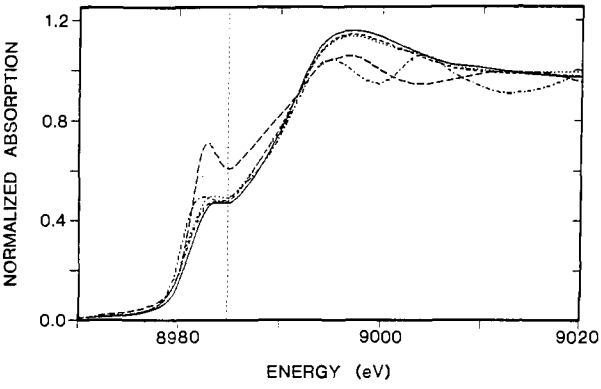


**Figure 6.** Cu X-ray absorption K edges for reduced 1% (solid), 5% (short dash), and 10% (dot) Cu/ZnO catalyst samples compared with $Cu_2O$ (long dash) and metallic Cu (dot–dash). The vertical dotted line is at 8985 eV.

can come from a static disorder of the environment of the Cu sites in this heterogeneous system.

We have attempted to model the effects of a static disorder on the EXAFS spectra by including an additional shell of Zn atoms in the fit of the Fourier-filtered Cu–Zn feature at 2.8 Å (non-phase-shifted) using Debye–Waller factors fixed from those of ZnO. The fit was improved by the addition of this second shell (resulting in 2.5 Zn at 3.29 Å, 1.4 Zn at 3.48 Å; the $F$ value decreased from 0.27 to 0.15, where $F = \{\sum[k^6(\text{data-fit})^2]/(\text{no. of points})\}^{1/2}$). With this simplified two-shell model for such static disorder, the total coordination number is 3.9, which is closer to the value of $12 \times {}^{8}/_{12} \times 67\% = 5.3$ expected from the edge analysis of surface sites. Note that as the Cu–Zn feature is being fit with parameters derived from Zn–Zn in ZnO, artifacts could arise from inadequacies in transferability.

**(B) Reduced Samples.** X-ray absorption edge spectra of metallic Cu and $Cu_2O$ were collected (Figure 5) for comparison with those of the reduced catalyst. Note that the positions of the preedge features of metallic Cu and $Cu_2O$ are quite similar at 8982 and 8983 eV, respectively, with some reduction in the intensity of the metallic Cu feature. However, the resonance features above the edge jump are different in that metallic Cu exhibits two peaks at 9004 and 9027 eV, while $Cu_2O$ has minima at these energies and a maximum at 9014 eV. Montano has studied the edges of small Cu microclusters, from dimers to 15-Å particles, and a representative edge is also reproduced in Figure 5.[21] When compared to Cu metal, the preedge transition looks very similar in intensity but the entire Cu edge is shifted by 1.4 eV to higher energy.[21] Alternatively, the two resonance features (at 8994 and 9004 eV) of bulk metallic Cu are not present in the Cu microcluster which exhibits a broad feature at 8999 eV. This difference in resonance features has been associated with the absence of fourth and higher shell atoms in the Cu microclusters.[21]

Edge data for the reduced catalyst samples are compared with metallic Cu and $Cu_2O$ in Figure 6. The absorption edge is shifted to lower energy after activation of the calcined catalyst (Figure 6 compared to Figure 1a), indicating the presence of either Cu(I) or Cu(0) (as metallic Cu or Cu microclusters). Due to the similarity of the edge spectra of metallic Cu, $Cu_2O$, and Cu microclusters, it is not straightforward to interpret these edge data. We can, however, first estimate the amount of metallic Cu and Cu microclusters present using EXAFS and then subtract this from the edge spectra in Figure 6 to obtain the difference edge spectra of the remaining Cu(I) phases (vide infra).

EXAFS data for the 1, 5, and 10% reduced samples were collected at room temperature (Figure 7a shows the EXAFS data for the 5% sample), and the FTs of these data are shown in Figure 7b. Curve-fitting analyses have been performed on these EXAFS data (Table II), and the resulting structural features (distances

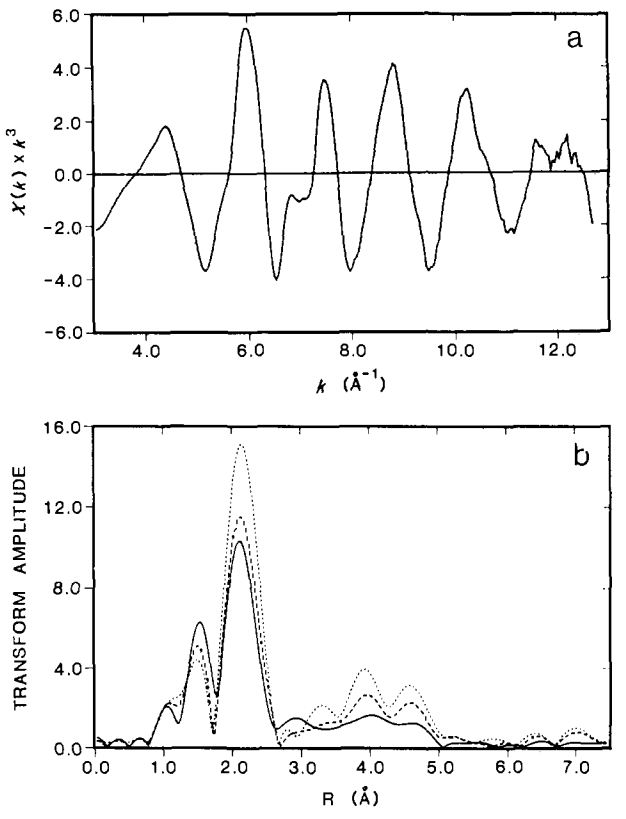


**Figure 7.** (a) EXAFS spectrum of 5% reduced Cu/ZnO catalyst. (b) Fourier transforms of the EXAFS of reduced 1% (solid), 5% (dash), and 10% (dot) Cu/ZnO over the $k$ range 3.8–12.1 Å$^{-1}$.

**Table II.** Curve-Fitting Results for Reduced Cu/ZnO Catalysts[a]

| Cu/ZnO sample, % | Cu–O $R$, Å (CN) | Cu–Cu 1st shell $R$, Å (CN) | coord no. ratios CuI/ CuM[b] | coord no. ratios OS/ CuM[b] | Cu–Cu 1st-shell residual[c] $R$, Å (CN) |
|---|---|---|---|---|---|
| 1 | 1.97 (2.2) | 2.53 (2.8) | 0.23 | 0.12 | 2.51 (1.5) |
| 5 | 1.94 (1.8) | 2.54 (3.1) | 0.27 | 0.18 | 2.52 (1.1) |
| 10 | 1.92 (1.6) | 2.54 (4.1) | 0.35 | 0.28 | 2.51 (1.0) |

[a] The unfiltered EXAFS data was first analyzed by 5-shell curve fitting (O shell and the 4 Cu shells in Cu metal); the percent of Cu foil contribution could be determined on the basis of the nearly constant ratios for the three outer shells to those of Cu foil (see text). Then, having fixed the percent Cu foil contribution, two additional shells were fit to determine the residual Cu present in the first Cu–Cu shell and in the Cu–O shell. [b] CuM = CN from fit of 4-shell features in FT of Cu metal EXAFS (12, 6, 24, 12 atoms in 1st, 2nd, 3rd, and 4th shells in Cu metal); CuI = CN from fit of first shell of Cu in catalyst; OS = CN from fit of 3 outer shells of Cu in catalyst. [c] After subtraction of corresponding Cu foil contribution (see text).

(21) Montano, P. A.; Shenoy, G. K.; Alp, E. E.; Schulze, W.; Urban, J. *Phys. Rev. Lett.* **1986**, *56*, 2076.

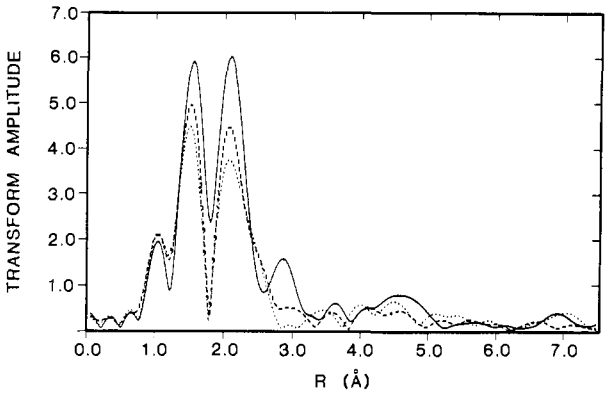


**Figure 8.** Fourier transforms over $k$ = 3.8–12.5 Å$^{-1}$ of the difference EXAFS spectra derived by subtraction of percent-weighted EXAFS of metallic Cu from the original EXAFS (*without renormalization*; see text for further details). Difference FTs from 1% (solid), 5% (dash), 10% (dot) reduced catalyst samples.

**Table III.** Distributions of Different Phases in the Reduced Cu/ZnO Catalysts[a]

| Cu/ZnO sample, % | Cu metal, % | 8-Å cluster,[b] % | oxide phase: Cu–O % | Cu–O $R$, Å (CN) | $Cu_2O$, % | Cu(I)/ZnO, % |
|---|---|---|---|---|---|---|
| 1 | 12 | 25 | 63 | 1.97 (3.5) | 20 | 43 |
| 5 | 18 | 19 | 63 | 1.94 (2.9) | 26 | 37 |
| 10 | 28 | 17 | 55 | 1.92 (2.9) | 26 | 29 |

[a] Curve fits performed as described in Table II. The percents of metallic Cu, Cu microclusters, and total Cu–O phase were derived from the curve-fitting results. The distribution within the Cu–O phase is based upon the edge analysis (see text for details). [b] Average CN = 6.

corrected for phase shifts) can be considered in three regions: (1) a Cu–O feature at 1.92–1.97 Å, (2) a Cu–Cu first-shell feature at ~2.54 Å, and (3) three outer Cu···Cu shell features (OS) at the same distances as those in bulk Cu metal (3.61, 4.42, and 5.11 Å). It is important to note that we find for all the reduced samples that the coordination number (CN) obtained for each of the three outer Cu–Cu shells to the analogous shell of pure Cu metal is essentially constant, which is not the case for the ratio of the first Cu–Cu shell. On the basis of the statistical calculation done by Greegor and Lytle,[22] the constant ratios of outer Cu···Cu shells in the activated catalysts to those in Cu metal indicate that these features are associated with large Cu clusters (>80 Å) which have an EXAFS amplitude similar to Cu metal. The ratio of the outer-shell amplitude of the catalyst to that of Cu foil (OS/CuM in Table II) gives an estimate of the percentage of metallic Cu present (12, 18, and 28% for the 1, 5, and 10% catalysts, respectively). The EXAFS of the metallic Cu can then be subtracted to obtain a residual EXAFS spectrum, the Fourier transform of which is shown in Figure 8.

Curve fitting analyses of these difference EXAFS data (Table II) indicate that there is a residual Cu–Cu feature for all three catalyst samples at ~2.51–2.52 Å, as well as a Cu–O feature at 1.92–1.97 Å. The residual Cu–Cu feature indicates that there are also Cu microclusters present in the reduced catalyst samples. Montano et al.[21] found that the first-shell Cu–Cu distance varies as a function of microcluster size. From Figure 4 of ref 21, the 2.51–2.52-Å Cu–Cu distance of the residual EXAFS spectra of these catalyst samples corresponds to an ~8-Å cluster diameter. Using the statistical calculation of surface atoms and surface sites on metal crystals done by Van Hardeveld and Hartog,[23] with the assumption of spherical geometry for the microcluster, the average first-shell coordination number for an 8-Å cluster is 6. The percentage of total Cu in the reduced catalyst in an 8-Å microcluster can then be calculated by dividing the CN of the Cu(residual) by this average CN of 6 (for example, for the 1% reduced sample, $^{1.5}/_{6}$ = 0.25). These estimates are given in Table III, column 3.[24]

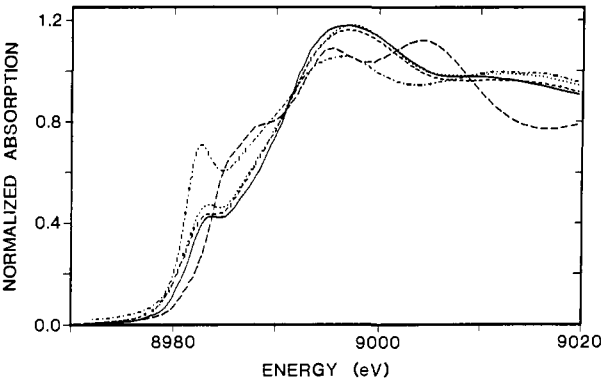


**Figure 9.** Difference Cu absorption K edge spectra, where the contributions of metallic Cu and Cu microclusters have been subtracted from the edge spectrum of reduced 1% (solid), 5% (short dash), and 10% (dot) Cu/ZnO samples. The residual Cu(I) phases are compared with edges of $Cu_2O$ (dot–dash) and 4-coordinate Cu(I) model, $Cu[N(CH_2CH_2\text{-}2\text{-}pyridyl)_3]BPh_4$[27] (long dash).

The remaining Cu–O feature at 1.92–1.97 Å should be due to a combination of a weak Cu–O contribution from these Cu clusters on oxide support sites and an oxide phase of Cu(I) ions. The Cu–O contribution of Cu metal particles on the support should be negligible due to the very small surface-to-bulk ratio.[25] The percentage of Cu in an oxide phase can be estimated as the percentage of Cu remaining in the catalyst after elimination of the metallic Cu and small Cu microcluster contributions. This percentage is given in the fourth column of Table III.

The CN of this oxide phase can then be obtained by dividing the CN of the first shell of oxygens in the EXAFS (Table II) by this percentage (for example, for the 1% activated sample, $^{2.2}/_{0.63}$ = 3.5). This is included in Table III (sixth column). From Table III, this coordination number is observed to decrease with increasing Cu doping. In addition, the Cu–O distance also decreases with increasing Cu concentration. This trend would seem to indicate that the Cu oxygen phase in the 1% catalyst is closer to ZnO where the coordination number is 4 and the M–O distance is 1.98 Å. The higher Cu concentration samples have structural parameters approaching $Cu_2O$, where the coordination number is 2 and the Cu–O distance is 1.85 Å. Thus the Cu–O phase appears to have contributions from both Cu/ZnO and $Cu_2O$, which vary with Cu doping concentration.

We can now further characterize the Cu(I) oxide phase in the reduced catalysts using the X-ray edges shown in Figure 6. The edges of metallic Cu and Cu microclusters (Figure 5) weighted by the percentages of these present in a given reduced catalyst sample (Table III) were subtracted from the reduced catalyst edge spectrum (in Figure 6) and the resulting spectrum renormalized. These difference edge spectra of the Cu(I) oxide phases are given in Figure 9. Since Cu(I) ion doped into the ZnO lattice should be in a 4-coordinate tetrahedral environment, it should not exhibit an 8983-eV preedge feature. Thus the 8983-eV peak in the difference spectrum of each of the three reduced catalysts indicates that there is a significant $Cu_2O$ component present. However, the normalized intensity of the 8983-eV feature in all reduced catalyst samples is decreased relative to that of $Cu_2O$. Therefore a Cu-doped ZnO phase is also required by this edge data. Using the edge spectra of $Cu_2O$ and a 4-coordinate Cu(I) model compound (both included in Figure 9), the relative amounts of these two components can be estimated as described for the difference edges of the calcined samples (last two columns in Table III).

(22) Greegor, R. B.; Lytle, F. W. *J. Catal.* **1980**, *63*, 476.
(23) Van Hardeveld, R.; Hartog, F. *Surf. Sci.* **1969**, *15*, 189.

(24) Note that a simplifying approximation is made here that any distribution of small clusters present is represented by an effective cluster size of 8 Å.
(25) Even assuming one O per Cu for all the Cu atoms in the microclusters, the Cu–O contribution averaged over all Cu sites is less than ca. 10% of the observed CN of 1.6–2.2 (see Tables II and III).

From this difference edge analysis there is 43%, 37%, and 29% Cu(I) ion doped in the ZnO lattice for the 1%, 5%, and 10% reduced catalysts, respectively.

We also note that as with the calcined catalyst, the difference EXAFS data of the Cu metal subtracted 1, 5, and 10% reduced catalysts (Figure 8) shows little intensity at 2.8 Å, where one would expect a significant contribution from Zn–Zn backscattering in the ZnO lattice. As the Cu(I) in the ZnO phase represents from $^{29}/_{72}$ to $^{43}/_{88}$ of the Cu contribution in these difference EXAFS spectra, this intensity again shows significant reduction. This reduction can be explained in terms of static disorder and possible population of surface sites as was described in subsection A for the calcined samples.

**Discussion**

The edge and EXAFS studies presented here demonstrate that for the calcined catalyst, in addition to bulk ZnO and CuO phases, there is also a significant amount of Cu(II) in a tetrahedral-like environment which is reasonably associated with Cu(II) doped into the ZnO lattice. This is apparent from the intensity of the 8986-eV absorption feature in the X-ray edge, which is relatively low, and indicates that about 75–47% of the Cu(II) is in non-tetragonal CuO sites for the 0.5–10% calcined samples. We and others have assigned this 8986-eV transition as a $1s \rightarrow 4p_z + L \rightarrow$ Cu(II) shakedown.[16,26] The energy of this transition will depend on ligand covalency, which affects the $L \rightarrow$ Cu(II) charge-transfer energy, and on the ligand geometry around the Cu(II), which influences the ligand field splitting of the 4p orbitals. As only oxide ligation need be considered in the catalyst, the lowered 8986-eV peak intensity must derive from the geometric effect on the 4p orbital set. An intense transition is present at 8986 eV in CuO and derives from the tetragonal site symmetry where the long axial O–Cu–O bond reduces the ligand field along the $z$ axis and leads to a $1s \rightarrow 4p_z$ transition at lower energy. In a tetrahedral ligand field all 4p orbitals are repelled to higher energy and a low-energy transition (at ~8986 eV) should be reduced in intensity. This behavior has been observed upon distortion of tetragonal to tetrahedral $CuCl_4^{2-}$.[20]

Other studies[11-13] have analyzed the Cu EXAFS of the calcined catalyst as indicating that there is no Cu doped into the ZnO lattice. This conclusion was based on the lack of the expected, relatively intense feature in the EXAFS FTs at about 2.8 Å, which would correspond to backscattering from the nearest neighbor Zn in the wurtzite lattice. For data collected at room temperature, there is clearly a peak above the noise level at about 2.8 Å. At 77 K, the appearance of strong features due to the outer shells of CuO dominate this region. However, this 2.8-Å peak in the room-temperature data is still greatly reduced in amplitude relative to what would be expected for about 50% Cu in ZnO sites. Since it is unlikely that Cu–Zn will have a significantly different scattering amplitude relative to Zn–Zn, an alternative explanation is required. It appears that a major contribution to this reduced intensity would occur from a static disorder of the Cu(II) site from the idealized $C_{3v}$ ZnO symmetry, perhaps due to the Jahn–Teller activity of this ion. In addition, if most of this Cu is at the ZnO surface, 4 out of 12 zinc ions will not contribute to the back-scattering.

For the reduced catalyst we find that four phases are present. First, bulk metallic Cu and $Cu_2O$ are clearly observed, as has also been reported by others.[5,8] Although there is some disagreement, neither phase is generally believed to be active in methanol synthesis. In addition, we find two components to be present in the dispersed phase, small Cu microclusters and Cu doped into the ZnO lattice. The small Cu clusters are required by the reduced amplitude of the outer-shell Cu foil features relative to the first-shell Cu–Cu scattering at 2.54 Å. Evidence for the presence of the Cu(I) in the ZnO lattice is more indirect; however, this is derived from a quantitative analysis of the edges. Subtraction of metallic Cu and small Cu microcluster contributions to the edge region results in the presence of a peak at 8984 eV. Our earlier studies on Cu(I) model complexes have led to the assignment of this peak as a $1s \rightarrow 4p$ transition whose energy is dependent on the geometry of the ligand field. In particular, $Cu_2O$, which has a linear two-coordinate structure, has an 8984-eV peak which corresponds to $1s \rightarrow 4p_{x,y}$ transition, the $4p_z$ being to higher energy due to repulsive interactions along the O–Cu–O bond. Again tetrahedral Cu(I) should not exhibit a low-energy $1s \rightarrow 4p$ transition as all 4p orbitals experience a repulsive interaction with the ligand set. For the reduced catalyst, the quantitative EXAFS analysis (Table III) allows us to estimate the total amount of Cu(I) sites present. On the basis of the known amplitude of the 8984-eV edge peak in $Cu_2O$, we find that only 32–47% (column 7/column 4; Table III) of the Cu(I) sites present in the reduced catalyst are in a $Cu_2O$ phase. The remaining Cu(I) does not exhibit a low-energy peak which would be consistent with a tetrahedral geometry and thus substitution into the ZnO lattice. Any EXAFS associated with the Cu(I)/ZnO site would not be observable over the intense outer-shell features of the metallic Cu and Cu microcluster sites, considering that the amplitude of the Cu–ZnO feature at 2.8 Å would likely be reduced as in the calcined catalyst due to static disorder and possible population of surface sites. Other EXAFS studies, which have focused on this region, have not observed Cu(I) in ZnO; however, it is the complementary quantitative edge analysis that indicates the presence of these sites. An additional trend in our data should be mentioned. As might be expected, decreasing the Cu concentration leads to an increase in the relative amount of Cu(I) in the ZnO lattice sites.

Both types of Cu site determined to be present in the dispersed phase have been suggested to be active in methanol synthesis. Our present studies on the powdered catalyst do not allow us to address the question of which are catalytically active. In addition, while the nonpolar surfaces are dominantly present in the <30% Cu/ZnO catalyst, the surface dependence of these sites cannot be determined from this work. We have, however, been able to create Cu(I) and small Cu cluster sites on the different single-crystal surfaces of ZnO and have studied their behavior for CO chemisorption using variable energy photoelectron spectroscopy (see the following paper). These studies demonstrate that $C_{3v}$ Cu(I) sites on the ZnO (0001) and (10$\bar{1}$0) surfaces are involved in high-affinity CO chemisorption which has been correlated with catalysis.[17]

**Acknowledgment.** We thank Haldor-Topsoe A/S for a generous gift of the calcined Cu/ZnO catalyst samples used in these studies and Dr. Britt Hedman for assistance with this work and preparation of the manuscript. This work was supported in part by Grant NSF CHE 85-12129 (to K.O.H.). Acknowledgment is also made to the donors of the Petroleum Research Fund, administered by the Americal Chemical Society, for support of this research (E.I.S.). Synchrotron radiation beam time was provided by the Stanford Synchrotron Radiation Laboratory, which is operated by the Department of Energy, Office of Basic Energy Sciences, Division of Chemical Sciences, and instrumentation was provided by the Division of Research Resources of the National Institutes of Health.

**Registry No.** Cu, 7440-50-8; ZnO, 1314-13-2.

(26) (a) Blair, R. A.; Goddard, W. A. *Phys. Rev. B* **1980**, *22*, 2767. (b) Kosugi, N.; Yokoyama, T.; Asakuna, K.; Kuroda, H. *Springer Proc. Phys.* **1984**, *2*, 55. (c) Kosugi, N.; Yokoyama, T.; Asakuna, K.; Kuroda, H. *Chem. Phys.* **1984**, *91*, 249.

(27) Karlin, K. D.; Hayes, J. C.; Hutchinson, J. P.; Hyde, J. R.; Zubieta, J. *Inorg. Chim. Acta* **1982**, *64*, L219.